J. Neural Eng. **6** (2009) 036003 (10pp) doi:10.1088/1741-2560/6/3/036003

A MEMS-based flexible multichannel ECoG-electrode array

Birthe Rubehn[1], Conrado Bosman[2], Robert Oostenveld[2], Pascal Fries[2] and Thomas Stieglitz[1]

[1] Laboratory for Biomedical Microtechnology, Department of Microsystems Engineering—IMTEK, University of Freiburg, Freiburg, Germany
[2] Donders Institute for Brain, Cognition and Behaviour, Radboud University Nijmegen, Nijmegen, The Netherlands

E-mail: Birthe.Rubehn@imtek.uni-freiburg.de

Received 12 February 2009
Accepted for publication 16 April 2009
Published 12 May 2009
Online at stacks.iop.org/JNE/6/036003

Abstract
We present a micromachined 252-channel ECoG (electrocorticogram)-electrode array, which is made of a thin polyimide foil substrate enclosing sputtered platinum electrode sites and conductor paths. The array subtends an area of approximately 35 mm by 60 mm and is designed to cover large parts of a hemisphere of a macaque monkey's cortex. Eight omnetics connectors are directly soldered to the foil. This leads to a compact assembly size which enables a chronic implantation of the array and allows free movements of the animal between the recording sessions. The electrode sites are 1 mm in diameter and were characterized by electrochemical impedance spectroscopy. At 1 kHz, the electrode impedances vary between 1.5 kΩ and 5 kΩ. The yield of functioning electrodes in three assembled devices is 99.5%. After implantation of a device with 100% working electrodes, standard electrocorticographic signals can be obtained from every electrode. The response to visual stimuli can be measured with electrodes lying on the visual cortex. After an implantation time of 4.5 months, all electrodes are still working and no decline in signal quality could be observed.

(Some figures in this article are in colour only in the electronic version)

1. Introduction

The brain is anatomically and functionally organized into separated regions. However, several studies support the notion that brain regions interact during information processing [1–3]. Thus, one of the major goals in neuroscience research is to determine the mechanisms that are responsible for neuronal interaction between several neuronal populations [4]. An interesting brain signal in the study of neuronal communication over large areas in the brain is the local field potential (LFP). The LFP is a measure of pre- and postsynaptic activity within a volume of neuronal tissue [5, 6]. Several studies showed that significant LFP modulations are related to sensory processing, motor planning, visuomotor interactions and higher cognitive functions such as attention, memory and decision making [7–13]. LFPs appear to convey relevant information that is not present in neuronal spike activity [10, 14, 15]. In addition, LFP fluctuations are also closely correlated with haemodynamic changes measured by functional magnetic resonance imaging (fMRI) [16] and underlie the generation of electroencephalographic (EEG) and magnetoencephalographic (MEG) measurements [17]. Thus, using techniques that are able to record LFP signals from large parts of the brain might help to understand the underlying mechanisms that allow the neuronal population interaction.

For that purpose, we developed a micromachined ECoG-electrode array which contains 252 electrode sites to cover large expanses of the cortex of a macaque's cortex. Electrode arrays made for recording electrocorticograms are already widely used in research as well as in clinical therapy. Besides understanding fundamental brain functions, scientists are interested in how brain signals can be used in therapy to treat neurological disorders such as paralysis by using brain–machine interfaces [18, 19]. In clinical practice,

ECoG-electrode arrays are implanted onto the cortex to locate the seizure focus during the pre-surgical diagnosis of epilepsy [20]. While in clinical practice commercially available arrays (Ad-Tech Medical Instrument Corporation, Racine, WI, USA) with electrode diameters and electrode pitches in the millimetre scale are used, researchers in medicine and engineering try to scale down the dimensions to micrometre size. This is in order to obtain a higher spatial resolution of brain signals from the cortex, which can be realized by using MEMS (microelectromechanical systems) technology. In the past few years, numerous groups presented precision-engineered or MEMS-based electrode arrays. With precision engineering, it is possible to reduce the dimensions of an electrode array. But implementing a large number of electrodes, that are individually connected to wires forming a bulky cable, leads to a large and rigid device which cannot be chronically implanted [21]. With MEMS-processing, it is easy to arrange a large number of microelectrodes inside a small area. But even most of the microarrays described in the literature do not have a larger number of electrodes, limited by the assembly. Even if the electrode array is processed on the wafer level, cables and connectors are still necessary to connect the electrodes to a measurement setup. Often microarrays are joined to printed circuit boards or to a bunch of cables making the microdevice bulky and rigid [22–25]. Most micromachined arrays have electrodes distributed over a small area with a small electrode pitch. Therewith, a high spatial resolution is obtained but the cortex region from which measurements can be taken is limited to the small array area [21–23]. If recordings over larger areas of the brain are needed, most micromachined arrays fail because they only cover a small brain area. In small animals, a micromachined electrode array can cover a rat's motor cortex [24] but cannot be used for larger cortex areas.

The array manufactured in this work has the electrodes equally distributed on a highly flexible substrate, which fits onto the cortex surface of a macaque's brain hemisphere. The electrode positioning is shown on a brain model made of MRI data (figure 1). Every dot represents a single electrode site, and the main sulci are highlighted with lines. We use MEMS technology not to produce very small electrodes sites with narrow electrode spacing but to arrange the large number of electrode sites, their cables and connectors on a flexible foil with reasonable dimensions to provide an electrode array which can be chronically implanted. While the electrode array covers an area of approximately 60 mm by 35 mm, the connector paths have to concentrate in a narrow ribbon cable which can be led through a small opening in the skull. Figure 2 shows a schematic diagram of the position of the foil on the cortex and the connectors on the skull while the latter is opened during implantation.

To circumvent a rigid assembly, both the array and the cable are processed on the wafer level as one device. Connectors are directly soldered to the thin cable after the lead through to minimize space requirements of the assembly. With this setup, only the flexible thin film array and cable are implanted whereas the larger connector part is fixed on the outside of the skull where it can be connected to a recording

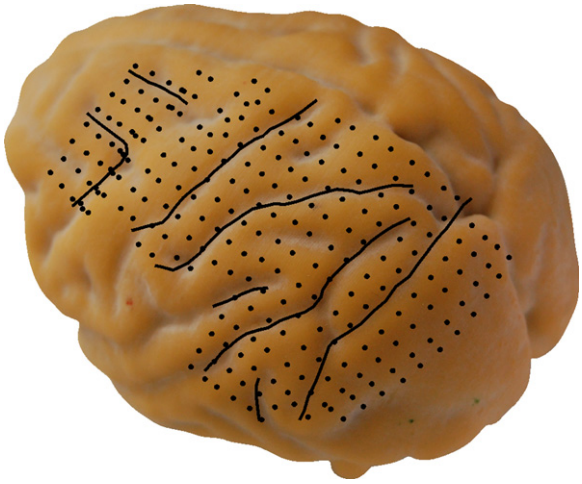

Figure 1. Three-dimensional plastic model of the macaque brain made by using MRI data (anterior left, posterior right). The main sulci are highlighted with lines. The dots represent the position of every single electrode site of the array.

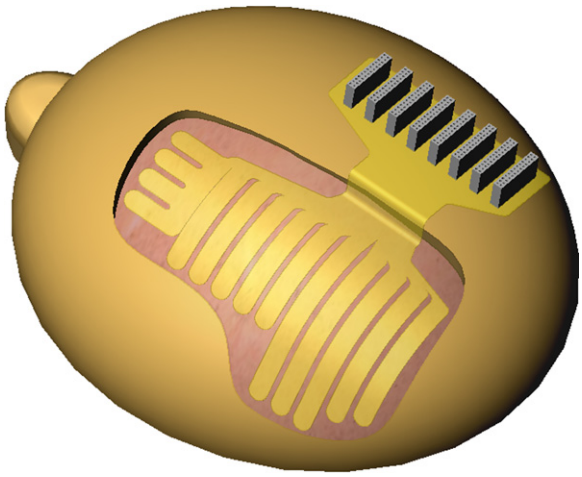

Figure 2. Schematic diagram of the flexible foil and its position. The head is facing to the left, the skull over the left hemisphere is opened and the polyimide foil is placed on the cortex while the connector part is fixed on the outside of the skull.

system. Even though the process of fabricating the polyimide foil is already presented elsewhere [26–28], this design and assembly introduce a new application for fundamental neuroscience and brain–computer interface-related studies.

2. Material and methods

2.1. Implant layout

The physiological requirements led to a layout of the ECoG-electrode array where 252 electrodes were distributed over 14 fingers (figure 3, right). The fingers were designed to fit exactly the brain cortical surface of a macaque monkey. Their design allows the adaption of the array to the cortex's curvature and to facilitate the implantation procedure by placing every finger individually. The conductor paths merged in 11 ribbon cables, which were mechanically separated from each other

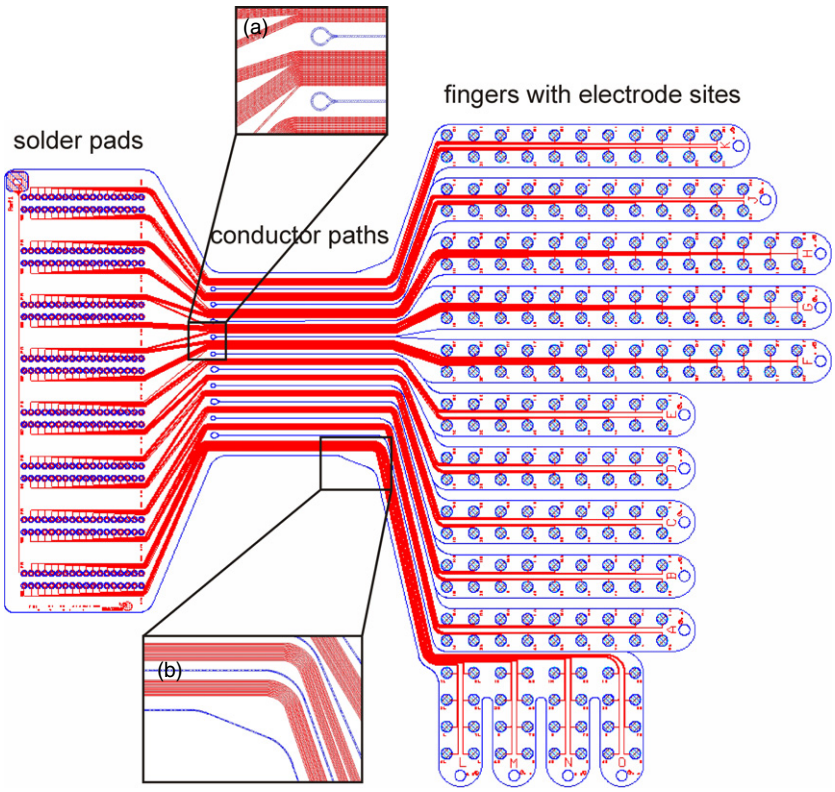

Figure 3. Layout of the ECoG-array with 252 electrodes on 14 fingers (right), the ribbon cable (middle) and solder pads (left).

to enhance flexibility (figure 3, middle). The electrodes have a diameter of 1 mm with electrode pitches of 2 mm, 2.5 mm and 3 mm, respectively. The connector paths have a width of 15 μm and a pitch of 30 μm; thus, MEMS technology is necessary to process and to integrate the high number of connector paths into the electrode array foil. The connector paths ended in solder pads to which eight Omnetics connectors (NPD series, Omnetics Connector Corp., Minneapolis, MN, USA) can be soldered by through-hole technology. To prevent the foil from tearing, the perimeters were designed to reduce mechanical stress at the notches (figures 3(a), (b)).

The substrate of the electrode array had to consist of a thin and flexible foil, which could adapt to the cortex's curvature. For this reason, polyimide was chosen as the substrate material. It was processed as a 10 μm thick foil on the wafer level using standard micromachining tools and processes. Apart from being thin and flexible, polyimide is mechanically strong so that a 10 μm thick foil can be handled and implanted without breaking.

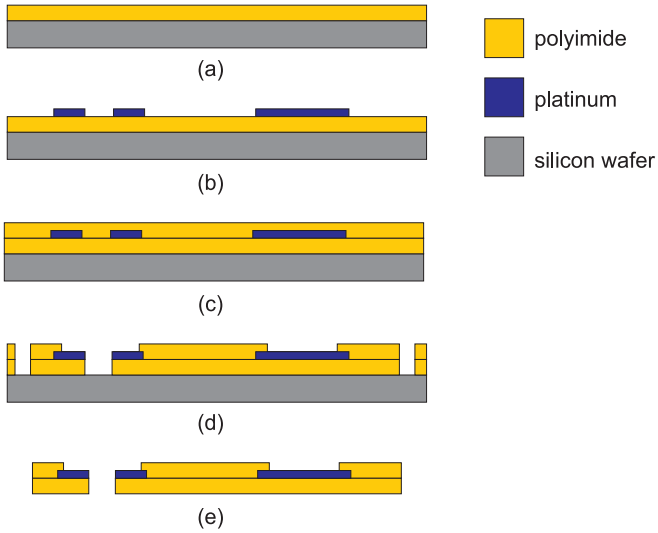

Figure 4. Process steps of the electrode array foil. (a) Polyimide is spin coated on the wafer; (b) platinum is sputtered and structured; (c) second layer of polyimide; (d) dry etching of electrode openings, solder pads and perimeters; (e) detaching the foil from the wafer.

2.2. MEMS processing

The electrode array was made by cleanroom processing. After cleaning a 4″ wafer with hydrofluoric acid for 15 s, the polyimide U-Varnish S (UBE, Tokyo, Japan) was spin coated at 3000 rpm for 30 s. To evaporate the solvent, the wafer was put on a hotplate for 3 min at 120 °C. Subsequently, the polyimide was cured under nitrogen atmosphere at 450 °C for 10 min (furnace: YES-459PB6-2PE-CP, Yield Engineering Systems Inc., San Jose, CA, USA) resulting in a 5 μm thick layer (figure 4(a)). Hexamethyldisiloxane (HMDS) was used as an adhesion promoter for the photoresist ma-N 1420 (Micro Resist Technology GmbH, Berlin, Germany) which was spin coated at 2700 rpm for 30 s. The 2.1 μm thick layer of photo resist was structured by exposing it to UV light (mask aligner: MA6, Süss MicroTec AG, Garching, Germany) through a chromium mask. After the development (development solution: ma-D 533 S, Micro Resist Technology

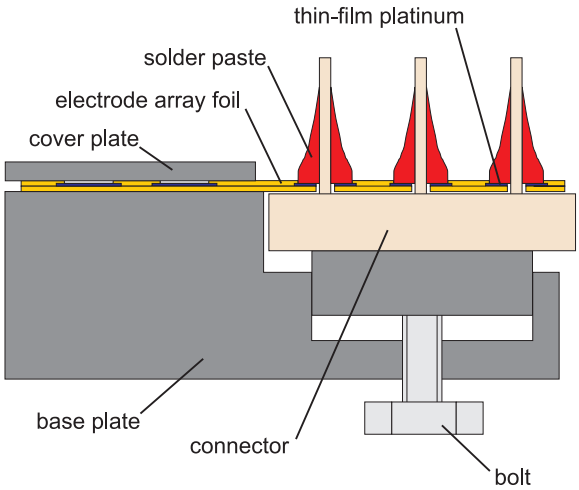

Figure 5. Soldering jig to hold the foil and the connectors in place while soldering.

GmbH, Berlin, Germany), the photoresist-free parts of the wafer defined the metal areas of the array. To improve the adhesion of the metal layer to the polyimide, the wafer was etched in an oxygen plasma (80 W, 30 mTorr; RIE Multiplex, STS, Newport, UK) for 30 s. Subsequently, a 300 nm layer of platinum was sputtered on the wafer (300 W, 7.5 min; Univex 500, Oerlikon Leybold Vacuum GmbH, Cologne, Germany). A lift-off step (immersion in acetone for 3 h including a 30 min ultrasonic treatment) removed the photoresist and the platinum on top of it. The platinum, which was directly sputtered onto the polyimide surface remained on the wafer and formed the electrode sites and the conductor paths (figure 4(b)). After activating the polyimide surface in the oxygen plasma, a second layer of polyimide was spin coated and cured (figure 4(c)). Two layers of the photoresist AZ9260 (MicroChemicals GmbH, Ulm, Germany) were spin coated at 1600 rpm for 30 s to form a layer of 28 μm. The photoresist was exposed and developed (AZ400 K, MicroChemicals GmbH, Ulm, Germany). It protected the underlying polyimide in the following etching step from the oxygen plasma (200 W for 10 min and 100 W for 25 min, 30 mTorr; RIE Multiplex). This etching step opened the electrodes and solder pads, and it defined the array perimeter by etching both polyimide layers down to the silicon wafer (figure 4(d)). After stripping the photoresist with acetone, tweezers were used to pull the device off the wafer (figure 4(e)).

2.3. Assembly and packaging

A custom-made soldering jig was developed to hold the polyimide foil and the connectors in place while soldering (figure 5). The base plate of the jig contained eight slots in which the connectors were inserted. A tapped through hole was located at the bottom of every slot, in which a bolt was placed. The foil was released from the wafer and put on the base plate. After aligning the foil to the underlying connectors, the latter were lifted by turning the bolts until the connector pins passed through the openings in the foil. A cover plate was mounted to the base plate to fixate the foil and shield it from solder and particles in the following soldering step.

Soldering paste (LFM-65X A75C, Almit GmbH, Michelstadt, Germany) was dispensed with a dispenser (DX-200, OKI International GmbH, Hochheim, Germany) through a dispensing tip with an inner diameter of 250 μm (blunt end stainless steel tips: I&J FISNAR, Fair Lawn, NJ, USA). The paste was soldered with a soldering iron at 250 °C. After removing the flux by rinsing the connector pins with acetone and isopropanol, epoxy (UHU plus endfest 300, UHU GmbH, Bühl, Germany) was applied on the pins, the solder, the polyimide foil and the connector bodies to fixate the components mechanically. After curing of the epoxy at room temperature for 24 h, the electrode array was released from the soldering jig.

2.4. Electrode characterization

To verify the functionality of the ECoG array, every electrode contact was characterized by electrochemical impedance spectroscopy with an impedance analyser (Solartron 1260 and 1287, Solartron Analytical, Farnborough, UK). A three-electrode setup with a platinum counter electrode and a silver/silver chloride reference electrode with 3 M KCl bridging electrolyte was used in Ringer's solution at room temperature. With a measuring amplitude of 10 mV, the impedance spectrum of the whole assembly was obtained between 1 Hz and 100 kHz, taking one measurement per decade. Impedance magnitude and phase were displayed in Bode plots.

The resistance of the conductor paths was extracted by contacting electrodes and solder pads with a needle prober, connected to a resistance meter (Multimeter 34401A, Agilent Technologies, Santa Clara, CA, USA).

The impedance between two neighbouring connector paths with a separation distance of 15 μm over a length of 40 mm was measured. The connector paths were immersed in 0.9 % saline solution while the electrode sites were kept dry. The impedance spectrum was measured by electrical impedance spectroscopy with the impedance analyser Solartron 1260 by applying a sine wave of 3 V amplitude, sweeping the frequencies from 1 Hz to 10 MHz. Additionally, the high-ohmic resistance between these two connector paths was measured with an electrometer (Keithley 6517A, Keithley Instruments Inc., Cleveland, OH, USA) by applying a dc voltage of -5 V to 15 V, measuring the current and calculating the resistance with a linear regression.

2.5. Implantation

All the surgical procedures reported in this study were approved by the animal ethical committee of the Radboud University, Nijmegen (DierExperimenten Comissie van de Radboud Universiteit, Nijmegen, RU-DEC-2004-151). One adult male Rhesus monkey (Macaca Mulatta) was trained to fix its eyes on a fixation point, located at the centre of a computer monitor at a 49 cm distance from the head. After fixing the central point, visual stimuli appeared. Stimuli were 4° diameter sinusoidal gratings (0.4–0.8 cycles/degree)

drifting unidirectionally within a circular aperture, located at approximately 4° eccentricity. One of the gratings was cued to be the target stimulus, and the monkey's task was to detect a small change in the orientation of the target grating to obtain reward. After reliable performance of the task, the monkey was subdurally implanted with the electrode array. Under general anaesthesia, a 6.5 cm by 4 cm craniotomy was performed using an Electric Pen Drive Neurospine 90 000 K (Synthes-Stratec, Solothurn, Switzerland) to expose the complete left hemisphere. The autoclaved (15 min at 134 °C and 2 bar) electrode array was placed subdurally over the left hemisphere. The boneflap was placed back and attached to the rest of the skull with calcium phosphate bone substitute and covered with dental acrylic.

2.6. Recordings

Recordings were started 3 weeks after the surgery. The signals from the 252 electrodes were amplified with a gain of 20 by a headstage amplifier (Headstage 32 V-G20, Plexon Inc., Dallas, TX, USA), low-pass filtered at 8 kHz and digitized at 32 kHz sampling frequency (Digital Lynx, 256 channels, Neuralynx Tucson, AZ, USA). The data were preprocessed and analysed off-line using the Fieldtrip toolbox (HTU http://www.ru.nl/neuroimaging/fieldtrip/UTH) for Matlab (The MathWorks, Inc., Natick, MA, USA). LFP activity was obtained by low-pass filtering at 200 Hz and downsampling to 1 kHz. To characterize the quality of the recorded signals, we performed a time-locked analysis and a power-spectral analysis. The time-locked analysis was performed over data epochs containing 35 consecutive stimulus presentations. Epochs were subsequently averaged over time. Power spectral estimation was calculated for each channel over 20 successive epochs of 3 s length. Each epoch was tapered using discrete prolate spheroidal sequences (Slepian functions) [29]. Spectral power was then computed as an average across epochs and tapers. This multi-taper method was used to optimize spectral concentration. In this analysis, tapering yielded a spectral concentration of ±1 Hz around each centre frequency.

3. Results

3.1. In vitro

The electrode array was successfully processed and assembled (figure 6). The soldering of the omnetics connectors to the polyimide foil led to a 99.5% yield of properly connected, functional electrodes in three assembled devices. The fixation of the soldered connections by epoxy made the array a robust device that could be handled easily during characterization and surgery. No damage of the array was observed during assembly, measurements or implantation. The connector part of the array attached on the outside of the skull fits into a volume of 42 mm by 20 mm by 10 mm. The electrochemical impedance spectrograms of all 252 electrodes located on one electrode array are shown in figure 7. Every grey curve represents the measurement data of one electrode site. The average value of all electrodes is the black curve.

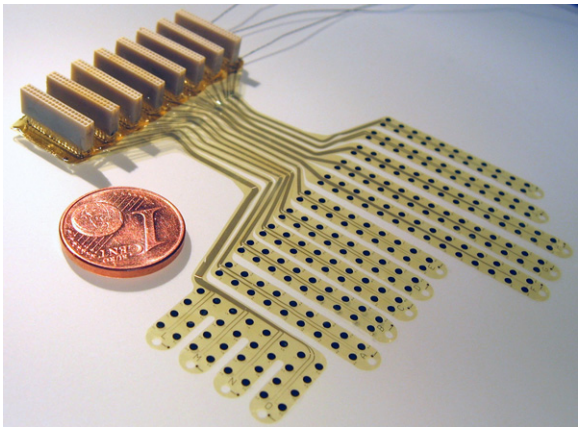

Figure 6. Fully assembled electrode array. The diameter of the coin is 16 mm.

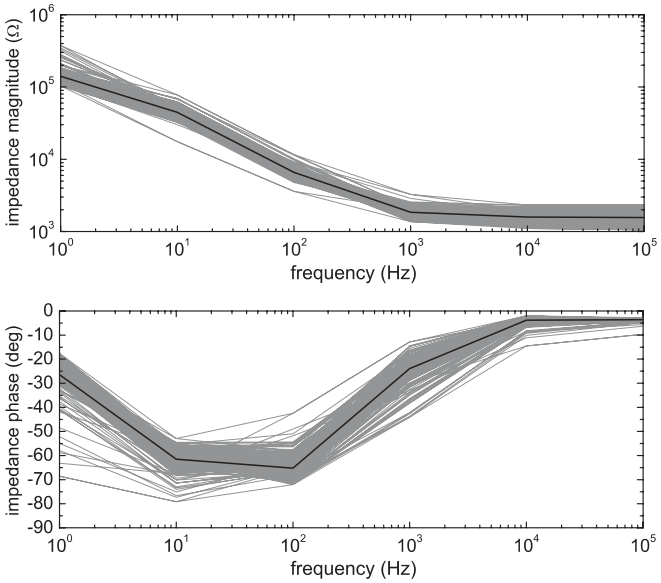

Figure 7. Impedance spectra of all 252 electrodes of the array. Grey lines represent single electrodes; the black line is the average of all electrodes.

The magnitude of the electrode impedances varied from 1.5 kΩ to 5 kΩ at 1 kHz. The resistances of the connector paths varied from 1 kΩ to 2 kΩ depending on the different connector paths' length. The cutoff frequency at which the impedance turned from a predominantly capacitive into a resistive behaviour was at 300 Hz. The impedance spectrogram of the electrode–electrolyte interface could be modelled with a basic electrical circuit model: an ohmic resistance parallel to a capacitor and both in series to a second ohmic resistance (figure 8). Fitting this model to the measured data of an exemplary electrode (software: Zview 2.8, Scribner Associates Inc., Southern Pines, NC, USA) resulted in $R_F = 143$ kΩ, $C_H = 377$ nF and $R_{AC} = 1.7$ kΩ, where R_{AC} was the access resistance to the electrode surface. This access resistance consisted of the resistance of the electrolyte as well as the resistance of the array's conductor paths. R_F and C_H represented the metal–electrolyte interface.

The electrical impedance spectrum of the impedance between two neighbouring connector paths was measured and

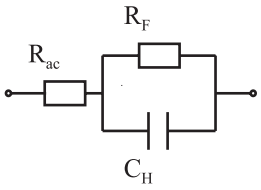

Figure 8. Basic equivalent circuit of an electrolyte–electrode interface.

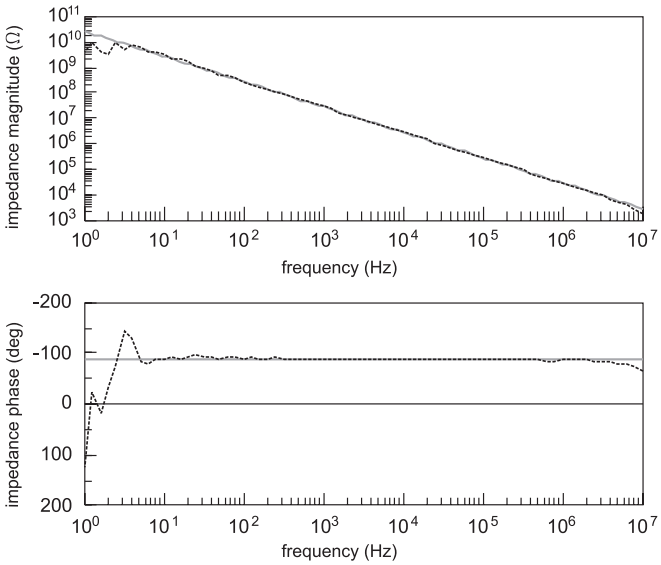

Figure 9. The electrical impedance spectrum of two neighbouring connector paths (single measurement) with the cable immersed in a saline solution while the electrodes were kept dry. The dashed line (black) shows the measurement and the solid line (grey) the simulation of a resistor (3.5 TΩ) and a capacitance (5.7 pF) in parallel.

showed a purely capacitive behaviour (figure 9, dashed black line). The impedance was modelled as a capacitor in parallel to an ohmic resistance. With Zview 2.8, this model was fitted to the measured spectrum between 250 Hz and 1 MHz because the Solartron 1260 can only measure resistances up to 100 MΩ. This value was achieved at 250 Hz so that the resistance values at frequencies below 250 Hz were larger. This fitting resulted in a capacitance of 5.7 pF with the resistance of greater than or equal to 100 MΩ. The dc resistance between the two connector paths was determined with Keithley's electrometer and resulted in a resistance of 3.5 TΩ, with the cable immersed in a saline solution. The simulation of the modelled impedance with 5.7 pF and 3.5 TΩ is shown in figure 9 (solid grey line).

To obtain ECoG signals with high amplitudes and low phase shifts during *in vivo* recordings, the input impedance of the headstage amplifier must be much higher than the electrode impedance. Figure 10 shows the impedance spectrum of Plexon's headstage HST/32 V-G20 (circles) and of the electrode with the highest measured impedance of the array (squares). The smallest ratio is found at 10 kHz where the input impedance is 1000 times higher than the electrode impedance.

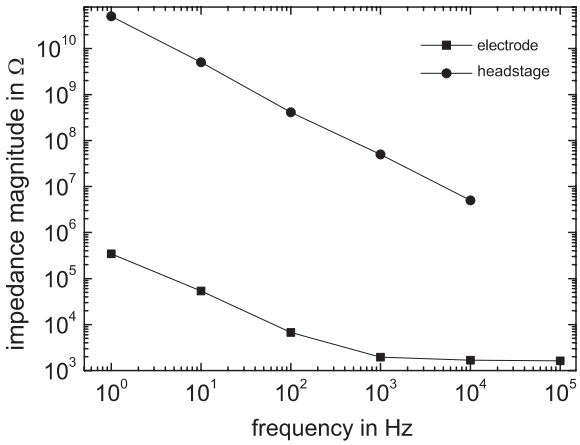

Figure 10. The magnitude of impedance as a function of frequency. The dots represent the input impedance of Plexon's headstage HST/32 V-G20 (data provided by the manufacturer). The squares are the measured electrochemical impedance magnitude of the array's electrode with the highest impedance.

3.2. In vivo

LFP signals were recorded from all electrodes while the monkey was awake and performing the visual task described in section 2.5. Figure 11(a) shows an example of 3 s of LFP activity observed from 12 out of the 252 channels distributed over the cortex. The exact position within the array is shown in the layout in figure 11(b). Every dot stands for an electrode site. Dots in red represent the displayed electrodes in figure 11(a). Channels numbered 1–12 are counted from anterior to posterior. Standard electrocorticographic signals were obtained from all electrodes. Figure 11(c) shows the power spectrum of all 252 electrodes for a 3 s epoch. Grey lines represent single electrodes whereas the black line shows the average power spectrum of all electrodes. The figure shows the two expected physiological peaks of power at low frequencies. The first peak, centred at 3 Hz, corresponds to delta–theta activity; the second one, centred at 18 Hz, represents the beta band. In figures 12 and 13, signals are plotted across the implantation time to evaluate the long-term performance of the electrodes. In figure 12(b), time 0 s in each graph is the onset of the visual stimulus. The response to a stimulus was measured with the same electrode (highlighted in figure 12(a)) 1, 2, 3 and 4 months after implantation. The black line shows the time-locked average over 35 trials from the same measurement session whereas the grey lines represent the 35 single trials. In the signals of all electrodes, two physiological relevant frequency bands could be found as peaks in the power spectrum (figure 11(c)). The power of the delta–theta (2–8 Hz), beta (15–25 Hz) and, in addition, alpha band (8–13 Hz) was calculated for a 3 s epoch in each measurement session and plotted over the implantation time (figure 13(a)). Every grey line represents the power of one single electrode. The mean value of 252 electrodes with the standard deviation is depicted in black. The power of the three frequency bands remained stable over time. To evaluate the quality of visual-evoked potentials over time, the maximum signal amplitude of an evoked potential (figure 13(b), squares) and the noise

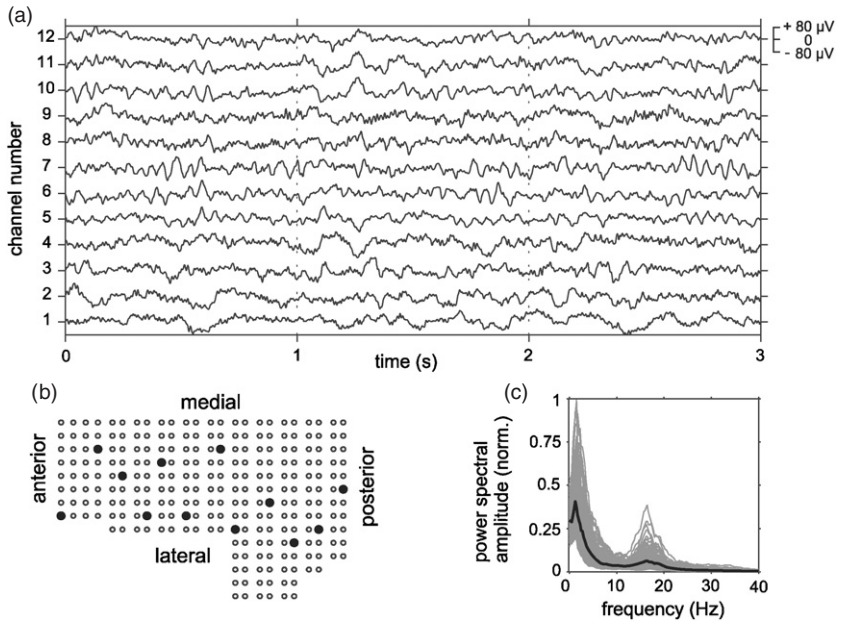

Figure 11. (a) Example of 3 s of local field potential (LFP) activity observed in 12 of the 252 channels of the ECoG-electrode array. LFPs were recorded in an awake monkey during the performance of a visual task. (b) Layout of the ECoG-electrode array; bold dots show the electrodes chosen for displaying in (a) (from anterior to posterior, channel numbers 1–12). (c) The power spectrum (Fourier multitaper estimation, 3 s window length, five tapers) of 252 channels is plotted in grey and the average value in black.

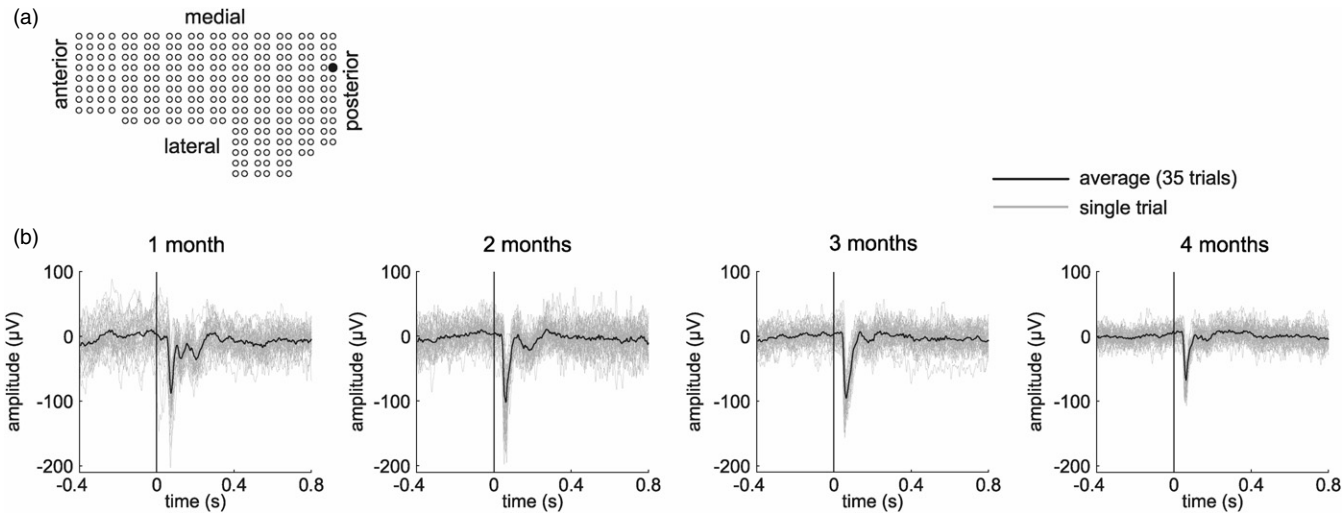

Figure 12. (a) The bold dot on the electrode array layout shows the selected channel. (b) Comparison between average and single trials of stimulus−locked LFPs after implantation surgery. Time 0 s in each graph represents the onset of the stimulus (4° sinusoidal grating). The grey lines represent 35 single trials. The black line shows the average over the 35 trials. The sessions were recorded after 1, 2, 3 and 4 months after implantation surgery.

(figure 13(b), triangles) were calculated from the signals of 46 electrodes located on the visual cortex area *V*1 (figure 1, the first four columns of electrodes counted from posterior). Due to the fact that not all cortex areas respond with an evoked potential to a visual stimulus, the noise of each electrode was calculated to obtain a measure of the performance of all electrodes. The dots (figure 13(b)) represent the mean of 252 electrodes with the standard deviation as error bars. The maximum signal amplitude was the maximum voltage in an interval of 50–100 ms after the stimulus onset. As a measure of variance, the noise was defined as the standard deviation of the measured signal before the stimulus onset. Both values were calculated from the data of a single trial. The mean of 35 trials obtained in one measurement session was calculated for each electrode. The values shown in figure 13(b) represent the mean and the standard deviation calculated from the values of 46 and 252 electrodes, respectively. The values were recorded in ten measurement sessions 0.75–4.5 months after implantation surgery. While the maximum signal amplitude was changing due to varied stimulation parameters in different sessions

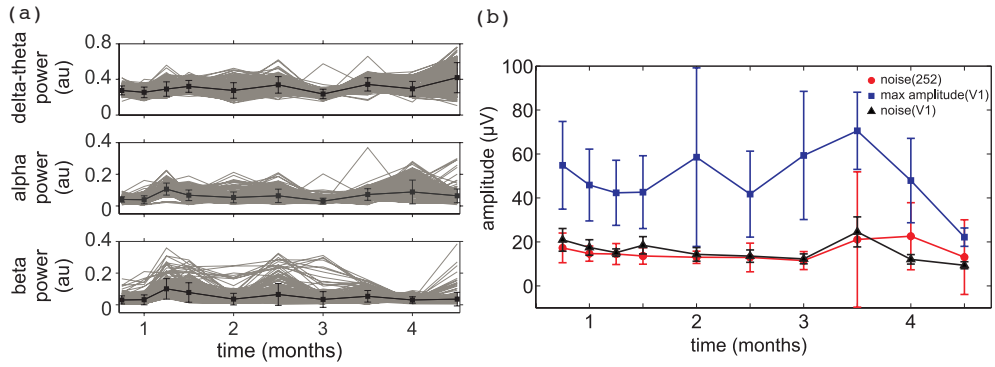

Figure 13. Signal stability over time: (a) The development of the beta (15–25 Hz), alpha (8–13 Hz) and delta–theta (2–8 Hz) band power over implantation time. Grey lines represent the 252 single electrode signals; the mean value of all electrodes with standard deviation is depicted in black. (b) Squares show the maximum signal amplitude of a visual-evoked potential; the triangles show the noise before stimulus onset. Both graphs display the mean value and the standard deviation of 46 electrodes located on the visual cortex area *V*1. The dots represent the noise before stimulus onset of all electrodes. The mean value of 252 electrodes with standard deviation is depicted.

(in the sessions at 2, 2.5 and 4.5 months, the stimulation parameters differed from the parameters in the other sessions), the noise remained stable over time.

4. Discussion

The presented wafer-level manufactured ECoG-electrode array combines a large number of electrodes distributed over a relatively large area with integrated micromachined cables. This reduced the assembly process to the soldering of the connectors to the array. In contrast to Huang *et al* [30] who connected a parylene-based micromachined ribbon cable to an omnetics connector by gluing it with conductive epoxy, the soldering process is more robust, easier to apply and thus more suited for a high-channel connection. Due to this single assembly step, the implanted part of the device remains thin and flexible and consists only of the micromachined foil made of the biocompatible materials polyimide and platinum [31–33] without any assembled adapter parts. The connector part of the array, containing the solder and the epoxy that were not tested for biocompatibility, was fixed on the outside of the skull. It was embedded in dental acrylic; thus, the solder and the epoxy were not in contact with the body. The connector part was made small enough to fit on a macaque monkey's head. By integrating the omnetics connectors, the array can be directly connected to a neurophysiologic standard recording system (Headstage 32 V-G20, Plexon Inc., Dallas, TX, USA).

The electrode diameter was chosen to minimize the impedance but it still supports the density of the electrode grid required to provide a high spatial resolution. In order to obtain a dense grid of electrodes over the cortex of a complete hemisphere, 2 mm was chosen as the minimum electrode pitch. This was limiting the electrode to 1 mm. In comparison with commercially available electrode arrays used in clinical diagnosis (e.g. Ad-Tech Medical Instrument Corporation, Racine, WI, USA), the impedance of our electrodes is higher. At 1 kHz, we measured a minimum of 1.5 kΩ whereas the Ad-Tech grid electrodes had an impedance magnitude of about 400 Ω at 1 kHz [34]. However, the Ad-Tech grid had a larger electrode pitch (5 mm), an about five times larger electrode area (electrode diameter: 2.3 mm), a lower number of electrodes (64) and a thicker substrate material (2 mm). Therefore, it was not suitable for chronic high-channel ECoG measurements in animal neurophysiology. On the other hand, our electrode array combined a high number of electrodes with a thin foil substrate. Compared to other micromachined electrodes (5–10 kΩ [24], 40–160 kΩ [21] and 330 kΩ [23], all at 1 kHz), our electrodes provided a lower impedance, which helped to measure high quality LFP signals on the cortex (figure 12).

An impedance spectrum of two neighbouring connector paths was measured and fitted to a capacitance (5.7 pF) with a resistor (3.5 TΩ) in parallel to it. These values show that the connector paths produce virtually no crosstalk when connected to biosignal amplifiers. These amplifiers have a maximum input impedance of some GΩ which is small compared to the impedance of the two neighbouring connector paths. This indicates that a neural signal measured on a neighbouring connector path is not originating from crosstalk inside the electrode array but from the conductivity of the biological tissue between the neighbouring electrode sites.

As discussed by Nelson [35], the ratio between the headstage's input impedance and the electrode impedance is crucial for an error-free recording of neural signals. The headstage impedance is at least three orders of magnitude higher than the electrode impedance (figure 10). Thus, the ratio had no effect on the measured signal which was not attenuated or distorted in the range of interest.

Exemplary signals from 12 electrodes lying on different cortex areas showed normal ECoG characteristics (figure 11(a)). Furthermore, the power spectrum of each channel contained peaks at physiological frequency bands (theta band and beta band in figure 11(c)), whose power stayed stable over the implantation time (figure 13(a)). This indicated that all electrodes, while put on different cortex areas, had a good contact to the underlying tissue and thus were able to obtain neural signals during the course of 4.5 months.

So far, there was no decline in signal quality over time. Signals obtained from visual-evoked potentials remained in

the same order of magnitude and the noise did not change over months (figures 12 and 13(b)).

5. Conclusion

One of the ultimate goals of neuroscience research is the understanding of the mechanisms through which brain regions are able to interact with each other in order to process information and produce behaviourally relevant responses [4]. Recent advances in multielectrode techniques have provided new insights in that direction [36, 37]. In this sense, the presented multielectrode array provides two relevant characteristics. Firstly, a large number of electrodes combined with the flexibility of a thin-film array allow the simultaneous recording over several brain areas. This electrode array is able to record neuronal activity from early visual areas (e.g. *V*1) to prefrontal regions, such as the frontal eye fields. This extensive sampling over large brain areas can help to reveal the mechanisms of interaction between neuronal populations during the development of a cognitive task. Secondly, signal fidelity recorded over time provides an indication that neuroprosthetic devices could be developed using ECoG-electrode arrays as the neural interface [13].

Acknowledgment

We would like to thank Dr Martin Schuettler for valuable discussions and consultations.

References

[1] Varela F, Lachaux J-P, Rodriguez E and Martinerie J 2001 The brainweb: phase synchronization and large-scale integration *Nat. Rev. Neurosci.* **2** 229–39
[2] Engel A K, Fries P and Singer W 2001 Dynamic predictions: oscillations and synchrony in top-down processing *Nat. Rev. Neurosci.* **2** 704–16
[3] Mesulam M-M 1998 From sensation to cognition *Brain* **121** 1013–52
[4] Fries P 2005 A mechanism for cognitive dynamics: neuronal communication through neuronal coherence *Trends Cogn. Sci.* **9** 474–80
[5] Mitzdorf U 1985 Current source-density method and application in cat cerebral cortex: investigation of evoked potentials and EEG phenomena *Physiol. Rev.* **65** 37–100
[6] Katzner S, Nauhaus I, Benucci A, Bonin V, Ringach D and Carandini M 2009 Local origin of field potentials in visual cortex *Neuron* **61** 35–41
[7] Henrie J A and Shapley R 2005 LFP power spectra in V1 cortex: the graded effect of stimulus contrast *J. Neurophysiol.* **94** 479–90
[8] Kreiman G, Hung C P, Kraskov A, Quiroga R Q, Poggio T and DiCarlo J J 2006 Object selectivity of local field potentials and spikes in the macaque inferior temporal cortex *Neuron* **49** 433–45
[9] Liu J and Newsome W T 2006 Local field potential in cortical area MT: stimulus tuning and behavioral correlations *J. Neurosci.* **26** 7779–90
[10] Womelsdorf T, Fries P, Mitra P P and Desimone R 2006 Gamma-band synchronization in visual cortex predicts speed of change detection *Nature* **439** 733–6
[11] Pesaran B, Nelson M J and Andersen R A 2008 Free choice activates a decision circuit between frontal and parietal cortex *Nature* **453** 406–9
[12] Pesaran B, Pezaris J S, Sahani M, Mitra P P and Andersen R A 2002 Temporal structure in neuronal activity during working memory in macaque parietal cortex *Nat. Neurosci.* **5** 805–11
[13] Scherberger H, Jarvis M R and Andersen R A 2005 Cortical local field potential encodes movement intentions in the posterior parietal cortex *Neuron* **46** 347–54
[14] Wilke M, Logothetis N K and Leopold D A 2006 Local field potential reflects perceptual suppression in monkey visual cortex *Proc. Natl Acad. Sci. USA* **103** 17507–12
[15] Womelsdorf T, Schoffelen J-M, Oostenveld R, Singer W, Desimone R, Engel A K and Fries P 2007 Modulation of neuronal interactions through neuronal synchronization *Science* **316** 1609–12
[16] Logothetis N K, Pauls J, Augath M, Trinath T and Oeltermann A 2001 Neurophysiological investigation of the basis of the fMRI signal *Nature* **412** 150–7
[17] Lopes das Silva F and Van Rotterdam A 1982 Biophysical aspects of EEG and MEG generation *Electroencephalography: Basic Principles, Clinical Applications and Related Fields* ed E Niedermeyer and F Lopes da Silva (Baltimore, MD: Lippincott Williams and Wilkins) pp 15–26
[18] Rickert J, Cardoso de Oliveira S, Vaadia E, Aertsen A, Rotter S and Mehring C 2005 Encoding of movement direction in different frequency ranges of motor cortical local field potentials *J. Neurosci.* **25** 8815–24
[19] Hochberg L R, Serruya M D, Friehs G M, Mukand J A, Saleh M, Caplan A H, Branner A, Chen D, Penn R D and Donoghue J P 2006 Neuronal ensemble control of prosthetic devices by a human with tetraplegia *Nature* **442** 164–71
[20] Schramm J and Clusmann H 2008 The surgery of epilepsy *Neurosurgery* **62** 463–81
[21] Tsytsarev V, Taketani M, Schottler F, Tanaka S and Hara M 2006 A new planar multielectrode array: recording from a rat auditory cortex *J. Neural. Eng.* **3** 293–8
[22] Kitzmiller J, Beversdorf D and Hansford D 2006 Fabrication and testing of microelectrodes for small-field cortical surface recordings *Biomed. Microdevices* **8** 81–5
[23] Takahashi H, Ejiri T, Nakao M, Nakamura N, Kaga K and Herve T 2003 Microelectrode array on folding polyimide ribbon for epidural mapping of functional evoked potentials *IEEE Trans. Biomed. Eng.* **50** 510–6
[24] Molina-Luna K, Buitrago M M, Hertler B, Schubring M, Haiss F, Nisch W, Schulz J B and Luft A R 2007 Cortical stimulation mapping using epidurally implanted thin-film microelectrode arrays *J. Neurosci. Methods* **161** 118–25
[25] Hollenberg B A, Richards C D, Richards R, Bahr D F and Rector D M 2006 A MEMS fabricated flexible electrode array for recording surface field potentials *J. Neurosci. Methods* **153** 147–53
[26] Shamma-Donoghue S A, May G A, Cotter N E, White R L and Simmons F B 1982 Thin-film multielectrode arrays for a cochlear prosthesis *IEEE Trans. Electron. Dev.* **29** 136–44
[27] Boppart S A, Wheeler B C and Wallace C S 1992 A flexible perforated microelectrode array for extended neural recordings *IEEE Trans. Biomed. Eng.* **39** 37–43
[28] Stieglitz T, Beutel H, Schuettler M and Meyer J-U 2000 Micromachined, polyimide-based devices for flexible neural interfaces *Biomed. Microdevices* **2** 283–94
[29] Jarvis M R and Mitra P P 2001 Sampling properties of the spectrum and coherency of sequences of action potentials *Neural. Computat.* **13** 717–49
[30] Huang R, Pang C, Tai Y-C, Emken J, Ustun C, Andersen R A and Burdick J W 2008 Integrated parylene-cabled silicon probes for neural prosthetics *Proc. of the 21st IEEE Annual Conf. on MEMS* pp 240–3

[31] Richardson R R Jr, Miller J A and Reichert W M 1993 Polyimides as biomaterials: preliminary biocompatibility testing *Biomaterials* **14** 627–35

[32] Klinge P M, Vafa M A, Brinker T, Brandis T, Walter G F, Stieglitz T, Samii M and Wewetzer K 2001 Immunohistochemical characterization of axonal sprouting and reactive tissue changes after long-term implantation of a polyimide sieve electrode to the transected adult rat sciatic nerve *Biomaterials* **22** 2333–43

[33] Lago N, Yoshida K, Koch K P and Navarro X 2007 Assessment of biocompatibility of chronically implanted polyimide and plantinum intrafascicular electrodes *IEEE Trans. Biomed. Eng.* **54** 281–90

[34] Henle C 2008 Personal communication, Laboratory for Biomedical Microtechnology, University of Freiburg, Germany

[35] Nelson M J, Pouget P, Nilsen E A, Patten C D and Schall J D 2008 Review of signal distortion through metal microelectrode recording circuits and filters *J. Neurosci. Methods* **169** 141–57

[36] Miller E K and Wilson M A 2008 All my circuits: using multiple electrodes to understand functioning neural networks *Neuron* **60** 483–8

[37] Kipke D R, Shain W, Buzsaki G, Fetz E, Henderson J M, Hetke J F and Schalk G 2008 Advanced neurotechnologies for chronic neural interfaces: new horizons and clinical opportunities *J. Neurosci.* **28** 11830–8